JACS
JOURNAL OF THE AMERICAN CHEMICAL SOCIETY

COMMUNICATION

pubs.acs.org/JACS

Rational Design of 3D Dendritic TiO_2 Nanostructures with Favorable Architectures

Ziqi Sun,[†] Jung Ho Kim,[*,†] Yue Zhao,[†] Fargol Bijarbooneh,[†] Victor Malgras,[†] Youngmin Lee,[‡] Yong-Mook Kang,[‡] and Shi Xue Dou[†]

[†]Institute for Superconducting and Electronic Materials, University of Wollongong, Innovation Campus, Squires Way, North Wollongong, NSW 2500, Australia

[‡]Division of Advanced Materials Engineering, Kongju National University, 275 Budaedong, Cheonan, Chungnam, Republic of Korea

Supporting Information

ABSTRACT: Controlling the morphology and size of titanium dioxide (TiO_2) nanostructures is crucial to obtain superior photocatalytic, photovoltaic, and electrochemical properties. However, the synthetic techniques for preparing such structures, especially those with complex configurations, still remain a challenge because of the rapid hydrolysis of Ti-containing polymer precursors in aqueous solution. Herein, we report a completely novel approach—three-dimensional (3D) TiO_2 nanostructures with favorable dendritic architectures—through a simple hydrothermal synthesis. The size of the 3D TiO_2 dendrites and the morphology of the constituent nano-units, in the form of nanorods, nanoribbons, and nanowires, are controlled by adjusting the precursor hydrolysis rate and the surfactant aggregation. These novel configurations of TiO_2 nanostructures possess higher surface area and superior electrochemical properties compared to nanoparticles with smooth surfaces. Our findings provide an effective solution for the synthesis of complex TiO_2 nanoarchitectures, which can pave the way to further improve the energy storage and energy conversion efficiency of TiO_2-based devices.

Titanium dioxide (TiO_2) has been recognized as one of the most promising semiconductor materials for photovoltaic, photocatalytic, and sensing applications owing to its wide band gap, environmental friendliness, and low cost.[1] In most potential applications, the quality and structure of the nanoparticles will undoubtedly play the pivotal role in determining their functions.[2] With rising interest in engineering the morphology of semiconducting materials during the past decade, the performance of TiO_2-based devices is known to be affected by not only the electronic structure but also the shape and size of the TiO_2.[1,3−6] The movement of electrons and holes in semiconductor nanomaterials is primarily governed by the well-known quantum confinement, and the transport properties related to phonons and photons are largely affected by the size and geometry of the materials.[1−4] Research on the intrinsic morphology/size−property relationship has engendered an urgent need for adjustable synthetic strategies, where the particle size and morphology of materials can be precisely controlled with designed functionalities. Accordingly, various techniques have been developed to synthesize TiO_2 nanostructures in diverse forms, such as nanoparticles, nanowires, nanotubes, and nanosheets.[1,6−9] Despite the above-mentioned successful demonstrations, a new approach to the synthesis of TiO_2 nanostructure is essential to obtain a high surface area to volume ratio. Usually, the TiO_2 nanostructures synthesized by the hydrothermal method are conventionally regular nanoparticles with smooth surfaces, which lack sharp corners and edges, and thus also lack copious active sites for reaction on the surfaces.

Several key factors, such as the hydrolysis rate and the surfactant aggregation structure, can affect the morphology of wet-chemistry-synthesized oxide nanostructures.[10] The growth of 3D nanostructures of some oxides, such as SiO_2, ZnO, and SnO_2, was successfully achieved in the form of nanowire/-rod/-tube flower-like clusters via a wet-chemistry process.[10−12] It was demonstrated that 3D flower-like ZnO or SnO_2 nanostructure clusters possess superior electrochemical activity and even entirely novel reaction pathways when compared to the nanoparticles with smooth surfaces. However, TiO_2 nanostructures with complex morphology are relatively hard to synthesize by this sort of process, owing to the rapid hydrolysis rate of Ti-containing precursors in aqueous solution, especially when they are compared to the well-developed SiO_2, ZnO, and SnO_2.[10−12] Therefore, the synthesis of TiO_2 nanostructures with tunable morphology and size still remains a major challenge, particularly in designed complex configurations.

To circumvent these problems, we propose a strategic hydrothermal synthesis of 3D dendritic TiO_2 nanostructures with well-defined shape and size. The existence of a large number of sharp edges and corners in the obtained 3D dendritic structures is extremely important for improving the photochemical and catalytic performance of TiO_2. The key innovation in the present study for tuning the morphology and size of TiO_2 nanostructures is to control the hydrolysis rate of the TiO_2 precursors and the aggregation of surfactant by changing the composition and potential of hydrogen (pH) value of the reaction solution. In detail, the TiO_2 nanostructures were synthesized using a simple one-pot hydrothermal method: First, an aqueous titanium isopropoxide (TTIP) solution was prepared by mixing TTIP, hydrochloric acid, and cetyltrimethylammonium bromide (CTAB) in distilled water. The aqueous solution was then removed to an autoclave with an appropriate amount of ethylene glycol (EG), and urea was added in some cases. The ratios of aqueous TTIP

Received: September 7, 2011
Published: October 31, 2011

solution to EG ($TTIP_{aq}$:EG = 1:0, 1:1, 1:2, 1:3) were adjusted to control the hydrolysis rate of precursors and the aggregation structure of the surfactant. Urea was added as a slow-release basic reagent to adjust the pH value of the reaction solution. More specific details of the sample preparation can be found in the Supporting Information, and the samples synthesized with different compositions are summarized in Table S1. The 3D nanostructures fabricated in this study are of great interest due to not only their unique structural characteristics but also their remarkable electrical, chemical, and optical properties.

The phase purity and crystal structure of the obtained samples were examined by X-ray diffraction (XRD) and Raman spectroscopy. The results (Figure S1) demonstrate that all TiO_2 nanostructures are well-crystallized in the rutile phase.

Figure 1 presents scanning electron microscopy (SEM) images of the 3D dendritic TiO_2 nanostructures obtained under different synthesis conditions. First, Figure 1a−c shows the morphology of 3D TiO_2 dendrites obtained from a fully aqueous solution with a composition of $100H_2O$:7HCl:0.03CTAB:0.05−0.01TTIP as reference samples ($TTIP_{aq}$:EG = 1:0, corresponding to samples 1−3 in Table S1). With a decreasing molar ratio of TTIP precursor in aqueous solution, the diameter of the microspheres obviously decreased from 10 μm (0.05 mol of TTIP, Figure 1a) to 2.5 μm (0.03 mol of TTIP, Figure 1b) and then 1.8 μm (0.01 mol of TTIP, Figure 1c). However, the TiO_2 nanostructures synthesized in the fully aqueous solution were not homogeneous and intact, and the reproducibility was not very good. In particular, crack propagations are easily observed on the surfaces of these microspheres, and thereby, most of the microspheres break into individual nanorods (Figure 1a and Figure S2).

Second, the composition of the aqueous TTIP solution was fixed at $100H_2O$:7HCl:0.03CTAB:0.05TTIP, and the volume ratios of aqueous TTIP solution to EG were adjusted to 1:1, 1:2, and 1:3. With increasing EG content in the $TTIP_{aq}$+EG mixed solution, 3D dendritic TiO_2 nanostructures with fine nanoribbon building units were obtained (Figure 1d−f, samples 4−6 in Table S1). When $TTIP_{aq}$:EG = 1:1, the diameter of the dendritic microspheres was around 3.8 μm (Figure 1d), and their constituent nanostructures were in the form of sharp nanoribbons 10−20 nm in width (Figure S3). On further increasing the proportion of EG in $TTIP_{aq}$:EG to 1:2 and 1:3, the particle size decreased to around 1.5 μm, as shown in Figure 1e,f. The constituent nano-units were in the form of typical nanoribbons, and the width of the nanoribbons was around 50 nm. From the low-magnification images shown in Figure S3, the 3D dendritic TiO_2 microspheres with well-defined nanoribbon branches were well-dispersed in isolated particles. Generally, the nanostructures prepared with the addition of EG had a more homogenously distributed particle size and more uniform shapes than those synthesized in the fully aqueous solutions. Moreover, the synthesis of these monodisperse 3D TiO_2 dendrites features a good reproducibility.

To further modify the morphology, 5 mmol of urea was added into the $TTIP_{aq}$+EG mixed solutions that had the same compositions as those for preparing samples 4−6 (urea-added samples are samples 7−9 in Table S1). Very interestingly, the constituent nano-units of the 3D TiO_2 dendritic microspheres were changed from nanoribbons to nanowires by the introduction of urea. It is worth noting that the generated nanowires have uniform diameters along their lengths. A higher EG amount simultaneously leads to longer nanowires and smaller diameters of the 3D TiO_2 microspheres. Low-magnification

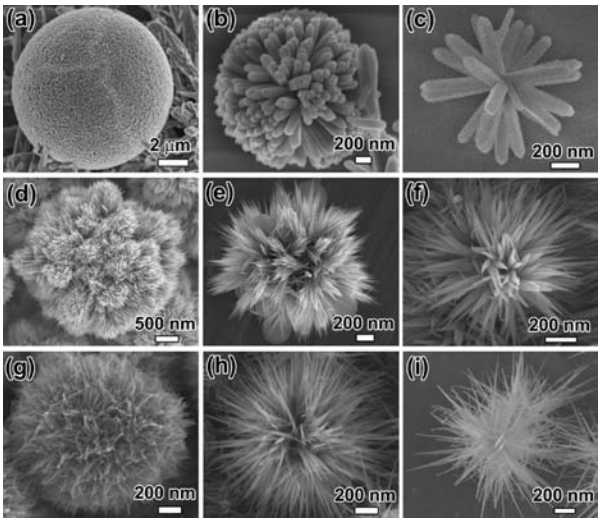

Figure 1. SEM images of 3D dendritic TiO_2 nanostructures: (a−c) 3D TiO_2 microspheres with nanorod building units obtained from aqueous TTIP solutions ($TTIP_{aq}$) having the composition of (a) $100H_2O$:7HCl:0.03CTAB:0.05TTIP (sample 1), (b) $100H_2O$:7HCl:0.03CTAB:0.03TTIP (sample 2), and (c) $100H_2O$:7HCl:0.03CTAB:0.01TTIP (sample 3). (d−f) 3D TiO_2 microspheres with nanoribbon building units obtained from mixed solutions of aqueous TTIP solution ($100H_2O$:7HCl:0.03CTAB:0.05TTIP) and EG: (d) $TTIP_{aq}$:EG = 1:1 (sample 4), (e) $TTIP_{aq}$:EG = 1:2 (sample 5), and (f) $TTIP_{aq}$:EG = 1:3 (sample 6). (g−i) 3D TiO_2 microspheres with nanowire building units obtained from mixed solutions consisting of aqueous TTIP solution ($100H_2O$:7HCl:0.03CTAB:0.05TTIP) and EG, as well as 5 mmol of urea: (g) $TTIP_{aq}$:EG = 1:1 (sample 7), (h) $TTIP_{aq}$:EG = 1:2 (sample 8), and (i) $TTIP_{aq}$:EG = 1:3 (sample 9).

images (Figure S4) of the 3D nanowire microspheres demonstrate uniform and monodisperse characteristics. The effects of the TTIP concentrations in the starting solution on the morphology of the 3D TiO_2 dendritic nanostructures were also considered. It was found that the TTIP concentration in the aqueous solution had a negligible influence on the morphology of the obtained TiO_2 nanostructures, except for the diameters of the microspheres. Figure S5 presents the morphology of 3D dendritic TiO_2 nanostructures synthesized from the solution with $TTIP_{aq}$:EG = 1:1, with the composition of the aqueous TTIP solution $100H_2O$:7HCl:0.03CTAB:0.3TTIP (sample 10). The constituent nanostructure of the 3D dendritic TiO_2 microspheres was still in the form of nanowires, but the diameters of the microspheres had grown to 4.8 μm, in contrast to 1.8 μm for the samples synthesized from the solution with 0.05 mol of TTIP. Thus, the size change promoted by the different ratios of $TTIP_{aq}$ to EG can also be realized by tuning the TTIP concentration in the starting aqueous solution.

To elucidate the microstructural origin of the growth mechanism, the constituent nano-units of the 3D TiO_2 dendrites obtained under different synthesis conditions were further investigated by high-resolution SEM and transmission electron microscopy (HRTEM). Figure 2a presents a high-magnification top view of typical nanorods obtained from the fully aqueous solution with 0.05 mol of TTIP (sample 1). The crystal structure and growth direction of the nanorods were then examined by HRTEM analysis together with the corresponding fast Fourier transform (FFT) patterns (Figure 2b,c). As evidenced by the HRTEM images, the nanorods are single crystals. The distance between adjacent

lattice fringes that run parallel to the nanorod wall was around 3.25 Å. This can be assigned as the interplane distance of (110) planes in the rutile structure. The distance between the fringes perpendicular to the wall, i.e., d = 2.96 Å, corresponds to the interplane distance of rutile (001) planes. The nanorods grown in the solution with a lower TTIP content had similar crystal structures. Therefore, the nanorod crystals of the 3D TiO_2 dendritic microspheres synthesized in the fully aqueous solutions grew along the [001] direction. The exposed surfaces of the nanorods are {110} facets.

Figure 2d−f presents the morphology and structure of individual nanoribbons. The enlarged SEM image (Figure 2d) clearly exhibits the nanoribbon feature of the nanostructures synthesized from the solution with a $TTIP_{aq}$:EG ratio of 1:2 (sample 5). The HRTEM images (Figure 2e,f) confirm that the nanoribbons are also single-crystal, and the lattice spacing parallel to the side wall is ∼3.25 Å, in accordance with the (110) planes of rutile TiO_2. Based on the analysis of FFT patterns and HRTEM fringes, the exposed surfaces of nanoribbons were determined to be {110} facets, and the growth direction of the crystals was along the [101] orientation. The variation of EG volume proportions in the reaction solutions did not affect the crystal growth direction of the nanoribbons.

Figure 2g−i shows the morphology and structure of the as-grown nanowires in 3D dendritic microspheres (sample 7). Both the SEM (Figure 2g) and TEM (Figure 2h) images indicate that the diameters of the nanowires are distributed in a narrow range, around 5 nm. The observed lattice fringes demonstrate that the growth of the nanowires was parallel to the (110) planes but perpendicular to the (001) planes. In other words, the growth direction of the nanowires in the 3D TiO_2 dendrites was in the [001] direction, which is the same as for the nanorods. The exposed surfaces of the nanowires were {110} facets.

It is interesting that the changes in the reaction solution compositions resulted in differences in the morphology of the 3D dendrites. These changes should be attributed to variations in the speed of the hydrolysis rate of the TTIP polymer precursors. During the hydrothermal process, the fully aqueous solution causes rapid hydrolysis and condensation rates of titanium hydrate, and thereby, the nano-units surrounding TiO_2 nuclei grow in the form of nanorods. In contrast, the nano-units tend to become nanoribbons when EG is introduced. Moreover, the 3D dendritic TiO_2 microspheres become more homogeneous and uniform. It has been reported that EG plays a major role in the hydrothermal process and assists in nanoribbon growth as "cosurfactant" and "cosolvent" in an aqueous system.[13] Moreover, the addition of EG can retard the hydrolysis rate of TTIP during the hydrothermal process.[14,15] Thus, the formation of nanoribbons should have resulted from the slowing down of the hydrolysis rate by the EG addition. Usually, only a slow hydrolysis of precursors could favor the formation of one-dimensional oxide nanostructures such as nanowires and nanorods.[10,15] When the reaction solutions were further modified by the addition of urea, the constituent nanostructures of the 3D TiO_2 dendrites changed to the form of nanowires. Urea is a weak Bronsted base and highly soluble in water. Its controlled hydrolysis at temperatures higher than 85 °C in aqueous solutions can yield ammonium cyanate and gradually, homogenously release OH^-.[16] The addition of slowly released urea can increase the pH of the reaction solution and retard the hydrolysis rate of TTIP during the hydrothermal process. Therefore, we can speculate that the hydrolysis rate of TTIP in the reaction solution is in the order of $TTIP_{aq}$ > $TTIP_{aq}$+EG > $TTIP_{aq}$+EG+urea, and leads to the crystal growth in the form of nanorods, nanoribbons, and nanowires, respectively.

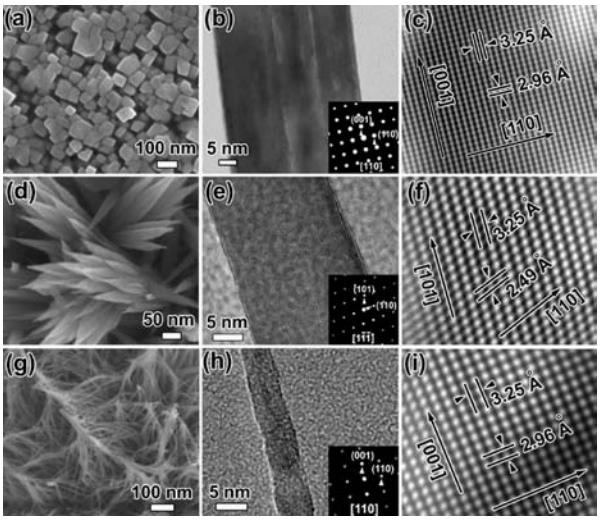

Figure 2. High-magnification SEM images and TEM characterizations of the building units of the 3D dendritic TiO_2 nanostructures in the form of nanorods, nanoribbons, and nanowires: (a) typical morphology of nanorods, (b) TEM image of one individual nanorod, and (c) HRTEM image of a nanorod viewed along the [110] direction; (d) typical morphology of nanoribbons, (e) TEM image of one individual nanoribbon, and (f) HRTEM image of nanoribbon viewed along the $[1\bar{1}1]$ direction; (g) typical morphology of nanowires, (h) TEM image of one individual nanowire, and (i) HRTEM image of nanowire viewed along the [110] direction. The insets in (b), (e), and (h) are the corresponding FFT patterns.

Besides the slowing of the hydrolysis rate of polymer precursor, the aggregation structure of surfactant in the solution with or without EG also contributes to the change in morphology. Wang et al. reported that the addition of polyethylene oxide−polypropylene oxide−polyethylene oxide (PEO-PPO-PEO) surfactant exceeding its critical micelle concentration does not favor the formation of dendritic Pt nanoparticles, because the PPO groups exist in the cores of micelles, while the hydrophilic PEO groups were exposed on the micelle surfaces.[17] In our study, the addition of EG tends to reduce the size and the total number of CTAB surfactant micelles dramatically by a "salt-in" effect, besides its effect toward slowing down the hydrolysis rate of precursor. As a result, some CTAB micelles would dissolve into individual molecules and adsorb on the TiO_2 seed surface, where they would act as template to form fine 3D dendritic morphologies from the mixed solution of $TTIP_{aq}$ and EG.

To help trace the growth process of diverse nanostructures and understand the related mechanism, two early-stage products obtained after 2 h at 80 and 120 °C were investigated by TEM (Figure S6). At the lower temperature, well-dispersed TiO_2 polyhedra and initially aggregated TiO_2 nanoclusters yielded from the complex precursor were observed to show sprouts in random directions (Figure S6a−c). As the reaction temperature further increased, the TiO_2 clusters grew significantly, and an early-stage dendritic morphology could be distinguished (Figure S6d). It is supposed that TTIP hydrolysis took place with water molecules to form titanium hydrates, and small TiO_2 growth centers (seeds) would be produced in the initial hydrothermal process (Figure S6b).

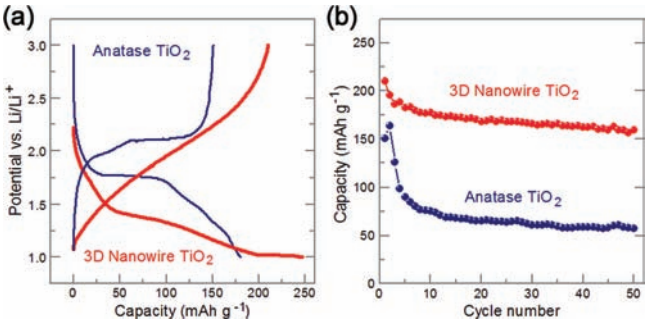

Figure 3. (a) First galvanostatic charge−discharge curves and (b) cyclic retention of the hydrothermally grown rutile 3D nanowireTiO_2 dendrites (sample 10) and anatase TiO_2 nanoparticle reference.

The hydrophobic groups of CTAB surfactants were then adsorbed on the surface of the TiO_2 seeds and guided the further growth of TiO_2 nanocrystals as templates (Figure S6c−e). Finally, by controlling the formation rate of titanium hydrates at the processing temperature, 3D dendritic TiO_2 nanostructures with tunable morphology and size can be obtained.

The surface areas of the 3D dendritic TiO_2 nanostructures were measured (Figure S7). The 3D nanowire TiO_2 dendrites which were synthesized from 100H_2O:7HCl:0.03CTAB:0.05TTIP aqueous solution together with 75 vol% EG ($TTIP_{aq}$:EG = 1:3) and 5 mmol of urea (sample 9) had a specific surface area of 97 $m^2 \cdot g^{-1}$, which is almost 2 times larger than that of the Degussa P25 nanoparticles (50 $m^2 \cdot g^{-1}$).

To explore the possibilities for electrochemical applications, the performance of 3D nanowire dendrites (sample 10) and anatase TiO_2 as anodes in lithium ion batteries was evaluated (Figure 3). The electrochemical reactivity of the 3D nanowire TiO_2 dendrites over the potential range of 1−3 V was tested up to the 50th cycle at a current of 0.1 C. The galvanostatic profiles of the anatase TiO_2 nanoparticles show a clear voltage plateau during Li^+ insertion/extraction, whereas the nanowire TiO_2 dendrites display the typical sloping voltage profiles of rutile phase, without any trace of a voltage plateau (Figure 3a).[18] Quite interestingly, most previous research has focused on anatase TiO_2, even though TiO_2 has various kinds of polymorphs, such as rutile, brookite, etc.[19] The preferential use of anatase phase compared to rutile phase for the lithium rechargeable battery is due not to the voltage plateau characteristic of anatase but to its better electrochemical performance (higher capacity and better cyclic retention). However, the 3D nanowire TiO_2 dendrites used in Figure 3a display the highest charge capacity, coming up to about 250 mAh $\cdot g^{-1}$, which has never been reported for any polymorph of TiO_2, as well as a superb initial Coulombic efficiency of around 85%. Figure 3b shows the cyclic retention of the nanowire TiO_2 dendrites and of the anatase nanoparticles. Even though the first discharge capacity of the anatase nanoparticles reaches 151 mAh $\cdot g^{-1}$, further cycling leads to drastic capacity decay to 57 mAh $\cdot g^{-1}$ after 50 cycles. Meanwhile, the 3D nanowire TiO_2 dendrites exhibit clear cyclic enhancement, possibly thanks to the morphological advantages for Li^+ storage. As pointed out by Park et al.,[19] 1D nanostructures such as urchin-like structures or nanorod structures on the surfaces of spherical particles can supply the most optimized environment for facilitating the charge/discharge process of Li^+ because of its amphoteric merits, including an appropriate surface area, excluding large irreversible capacity, and the high aspect ratio necessary for fast electron transport.

In summary, novel 3D dendritic TiO_2 nanostructures with tunable nanoscale building units were synthesized via a facile one-step hydrothermal synthesis method, based on a strategy of controlling the hydrolysis rate of the precursor and the aggregation of surfactant. The obtained 3D dendritic TiO_2 nanostructures have abundant sharp corners and edges and thus possess very high surface areas and dramatically improved electrochemical performance. The successful synthesis of complex TiO_2 nanostructures via a controllable approach, by introducing non-aqueous short-chain alcohol as cosolvent or cosurfactant, opens up a new way to synthesize TiO_2 nanomaterials and to improve the electrochemical performance of TiO_2-based devices.

■ ASSOCIATED CONTENT

Supporting Information. Preparation process, additional SEM and TEM images, XRD, Raman spectra, and specific surface area data. This material is available free of charge via the Internet at http://pubs.acs.org.

■ AUTHOR INFORMATION

Corresponding Author
jhk@uow.edu.au

■ ACKNOWLEDGMENT

This work was supported by Australian Research Council Discovery Project DP1096546. Z.S. was supported by an Australian Postdoctoral Research Fellowship.

■ REFERENCES

(1) Chen, X.; Mao, S. S. *Chem. Rev.* **2007**, *107*, 2891.
(2) Burda, C.; Chen, X.; Narayanan, R.; El-Sayed, M. A. *Chem. Rev.* **2005**, *105*, 1025.
(3) Liu, G.; Wang, L. Z.; Yang, H. G.; Cheng, H. M.; Lu, G. Q. *J. Mater. Chem.* **2010**, *20*, 831.
(4) Sun, C. H.; Yang, H. G.; Chen, J. S.; Li, Z.; Lou, X. W.; Li, C.; Smith, S.; Lu, G. Q.; Yang, H. G. *Chem. Commun.* **2011**, *46*, 6129.
(5) Alivisatos, A. P. *Science* **1996**, *271*, 933.
(6) Shankar, K.; Basham, J. I.; Allam, N. K.; Varghese, O. K.; Mor, G. K.; Feng, X.; Paulose, M.; Seabold, J. A.; Choi, K; Grimes, C. A. *J. Phys. Chem. C* **2009**, *113*, 6327.
(7) Yang, H. G.; Sun, C. H.; Qiao, S. Z.; Zou, J.; Liu, G.; Smith, S. C.; Cheng, H. M.; Lu, G. Q. *Nature* **2008**, *453*, 638.
(8) Liu, S.; Yu, J.; Jaroniec, M. *J. Am. Chem. Soc.* **2010**, *132*, 11914.
(9) Fang, W.; Zhou, J.; Liu, J.; Chen, Z.; Yang, C.; Sun, C.; Qian, G.; Zou, J.; Qiao, S.; Yang, H. *Chem.—Eur. J.* **2011**, *17*, 1423.
(10) Wan, Y.; Zhao, D. Y. *Chem. Rev.* **2007**, *107*, 2821.
(11) Zhang, Q.; Dandeneau, C. S.; Zhou, X.; Cao, G. *Adv. Mater.* **2009**, *21*, 4087.
(12) Wang, L.; Liu, X.; Lu, G.; Wang, Y. *Mater. Chem. Phys.* **2011**, *127*, 114.
(13) Zana, R. *Adv. Colloid Interface Sci.* **1995**, *57*, 1.
(14) Dong, R.; Hao, J. *Chem. Rev.* **2010**, *110*, 4978.
(15) Huo, Q. S.; Zhao, D. Y.; Feng, J. L.; Weston, K.; Buratto, S. K.; Stucky, G. D.; Schacht, S.; Schuth, F. *Adv. Mater.* **1997**, *9*, 974.
(16) Hu, M. Z. C.; Harris, M. T.; Byers, C. H. *J. Colloid Interface Sci.* **1998**, *198*, 87.
(17) Wang, L.; Yamauchi, Y. *J. Am. Chem. Soc.* **2009**, *131*, 9152.
(18) Kang, Y.; Go, J.; Lee, S. M.; Choi, W. *Electrochem. Commun.* **2007**, *9*, 1276.
(19) Park, J.; Kim, J.; Kwon, H.; Song, H. *Adv. Mater.* **2009**, *21*, 803.